Li Dayong (Orcid ID: 0000-0002-5739-7606)

Shi Yandong (Orcid ID: 0000-0002-5192-1091)

Experimental and Numerical Evaluations on the Effects of Adhesive Fillet, Overlap Length, and Un-bonded Area in Adhesive-bonded Joints

Guanghan Wu[a], Dayong Li[a,*], Wei-Jen Lai[b], Qiuren Chen[c], Yandong Shi[d], Li Huang[d], Shiyao Huang[b], Hongtae Kang[c], Yinghong Peng[a], Xuming Su[b]

[a]State Key Laboratory of Mechanical Systems and Vibration, Shanghai Jiao Tong University, Shanghai 200240, China

[*]E-mail: dyli@sjtu.edu.cn, Tel. 86-21-34206313

[b]Research and Innovation Center, Ford Motor Company, Dearborn, MI 48121, USA

[c]College of Engineering and Computer Science, University of Michigan-Dearborn, Dearborn, MI 48128, USA

[d]Materials and Process Research, Ford Motor Research and Engineering Center, Nanjing 211100, PR China

---

[*] Corresponding author.
E-mail address: dyli@sjtu.edu.cn (Dayong Li)

Abstract

To realize robust structural design, the effects of the adhesive fillet, overlap length, and un-bonded area in adhesive-bonded joints need to be fully understood and incorporated into a fatigue life estimation method. In the present work, both static and fatigue experiments are performed on six types of adhesive-bonded joints to illuminate these effects systematically. A straightforward total fatigue life evaluation method is proposed to address these effects. A statistical crack initiation model is established based on the fatigue data of bulk adhesive specimens. Growth life is calculated using the interfacial crack model and mixed mode crack growth method. Good correlation is observed between the calculated and experimental fatigue lives. Furthermore, the effects of the adhesive fillet, overlap length, and un-bonded area are analyzed based on both calculated and experimental results. Results indicate that adhesive fillet postpones crack initiation by reducing local strain level, both overlap length and un-bonded area change the growth life by length. Besides, overlap length promotes the fraction of mode II strain energy release rate in total, reducing crack growth rates and extending growth life.

Key words: adhesive fillet; overlap length; un-bonded area; crack initiation; local strain-stress approach; mixed mode crack growth.

1. Introduction

The outstanding mechanical properties of adhesive-bonded joints, e.g., lightweight, uniform stress distribution, watertight, excellent corrosion protection[1], enhanced noise, vibration and harshness (NVH) performance[2], the ability to join different materials[3,4], etc., lead to increasing use in joining complex auto body structures[5]. From the durability design's perspective[6], there is a specific need for analysis and design tools that can provide physical insight and characterize the effects of design variables.

Regarding the adhesive-bonded joints, the adhesive fillet, overlap length, and un-bonded area are the most widely used design variables which could significantly change the joint's durability performance[7,8]. Among the whole fatigue failure process, adhesive fillets have been identified as most contributing to extend crack initiation by reducing stress concentration at the interface corner between substrate and adhesive. By recording the back-face strain during tests and measuring the damage in different locations of adhesive-bonded joints, Solana and Crocombe[9] found that the damage in adhesive-bonded joints appeared first in the fillet. Removing the adhesive fillet will eliminate the initiation phase and consequently reduce the fatigue life[10]. Furthermore, the proportion of crack initiation life in total life has been found to vary in different types of specimens[11,12]. To establish crack initiation model, the intensity of the singular stress field[13,14] has been considered and transformed into the fatigue parameter[13,15] to correlate the test data. However, it is not widely used, especially for a cohesive failure crack. One of the possible reasons is that the stress singularity will be significantly changed by the round radius, which is created during the substrate cutting process.

3

Generally, the total fatigue failure of an adhesive-bonded joint consists of crack initiation [16,17] and subsequent crack growth[18–21]. It has been reported that the proportion of crack growth life will increase with increasing load levels[22–24]. At the same external load level, the fatigue life of joints with larger overlap length is longer than those with smaller ones, which can be attributed to longer crack growth length[25]. Jen and Ko[26] studied the effect of overlap length on the fatigue strength of epoxy adhesive-bonded aluminum single lap joints. Results indicate that fatigue resistance decreases with the decreasing overlap length. The un-bonded area is expected to have a similar effect of overlap length. By comparing the fatigue behavior of weld-bonded and adhesive-bonded joints[27,28], Xu et al.[28] found that at the same external load level, the fatigue life of weld-bonded joints is smaller than that of adhesive-bonded joints, especially at higher load levels. They found the adhesive was not bonded at the weld nugget area due to the burning of adhesive during nugget formation. However, these effects have not been characterized by existing fatigue models.

Fracture mechanism-based methods are commonly used to predict crack growth life. The crack growth laws in Mode I and Mode II are widely determined by using double cantilever beam (DCB) specimens[18–20] and 3-points end-notched flexure (3ENF) specimens[19], respectively. Crack growth life was calculated by integrating Paris law from an assumed initial crack to final failure. But the estimated results are not promising. One of the reasons is the complexity of loading conditions in adhesive-bonded joints. Most adhesives are under multi-axial stress conditions[21] in practice, e.g., peel, shear, and axial stresses in the adhesive layer, even for the simplest single lap joint[29], which bring challenges to growth life estimation. Furthermore, the crack initiation phase was omitted in these research studies, which would

4

lead to conservative predicted results[30]. By assuming the crack growth of the adhesive as a result of progressive material deterioration in the cohesive zone and the interaction thereof with the surrounding continuum[24,31], the cohesive damage model (CDM) was developed to simulate the entire failure process of adhesive-bonded joints. The location of crack initiation and growth are usually determined by utilizing a promising phenomenological criterion[32-34] based on the pure mode I and mode II values, which can be determined directly or inversely. Mesh sensitivity can also be avoided given an appropriate mesh refinement. But time-consuming computation is still inevitable due to the mesh refinement and sensitivity examination induced by stress singularity at the substrate edge.

In the present work, the effects of the adhesive fillet, overlap length, and un-bonded area are systematically illustrated in aluminum adhesive-bonded lap-shear joints. A total fatigue estimation method is proposed for the performance characterization by straightforwardly dividing the failure into crack initiation and growth. Crack initiation is modeled using the fatigue test data of bulk adhesive specimens fitted by the Manson-Coffin-Basquin equation. Local strain data obtained from detailed 3D FE models are used for the crack initiation site and life predictions. Crack growth life is calculated through the integration of crack growth rates as a function of strain energy release rates. The interfacial crack model is coupled with mixed mode crack growth model to capture the effect of mixed mode ratio. Finally, calculated results are compared and analyzed together with experimental results, well characterizing the effects of the adhesive fillet, overlap length, and un-bonded area.

5

2. Experiments

Both bulk adhesive specimens and adhesive-bonded joints are tested in this study. Fatigue test results of bulk adhesive specimens are used for crack initiation modeling. Quasi-static and fatigue tests on adhesive-bonded joints are used to illustrate the effects of adhesive fillet, overlap length and un-bonded area on crack initiation and growth.

2.1 Specimen preparation and test setup

The static and fatigue tests follow ISO527-2[35] and ASTM D-3166-99[36] for bulk adhesive specimens and adhesive-bonded lap-shear joints, respectively. Fig.1 shows the specimen configurations and dimensions for both specimens, where L is the overlap length and D is the diameter of the embedded PTFE tape (round shaded area) for the lap-shear joints. In order to study the effects of different geometric features, six types of lap-shear joints were produced with two types of adhesive fillets, three overlap lengths, and two tape diameters. Details of the joints are listed in Table 1. Fig.2 shows the geometries of the arc and full triangular fillets. The detailed dimensions will be shown later in section 2.2. The mechanical properties of the substrate and the cured adhesive are listed in Table 2. Alcoa 951[TM] pretreatment was adopted for AA6111-T4 to promote long-term corrosion resistance of the adhesive bond. The thickness of the adhesive layer in the joints was controlled by embedding 0.275 mm-diameter glass beads. As suggested by the supplier, the adhesive curing process was performed in an oven at 180℃ for 30 minutes.
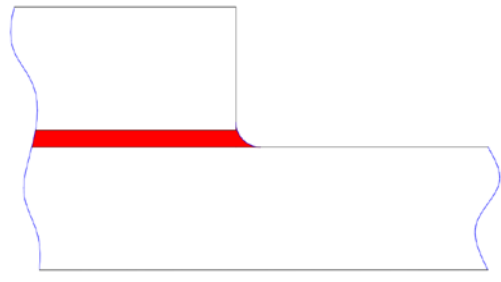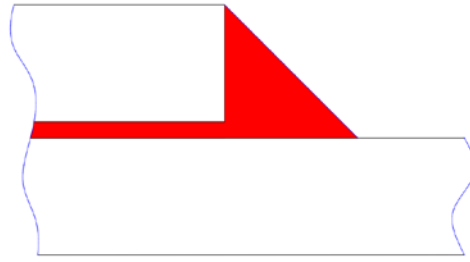
6
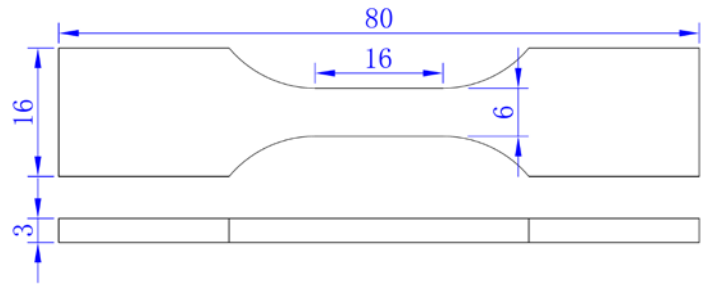
(a)
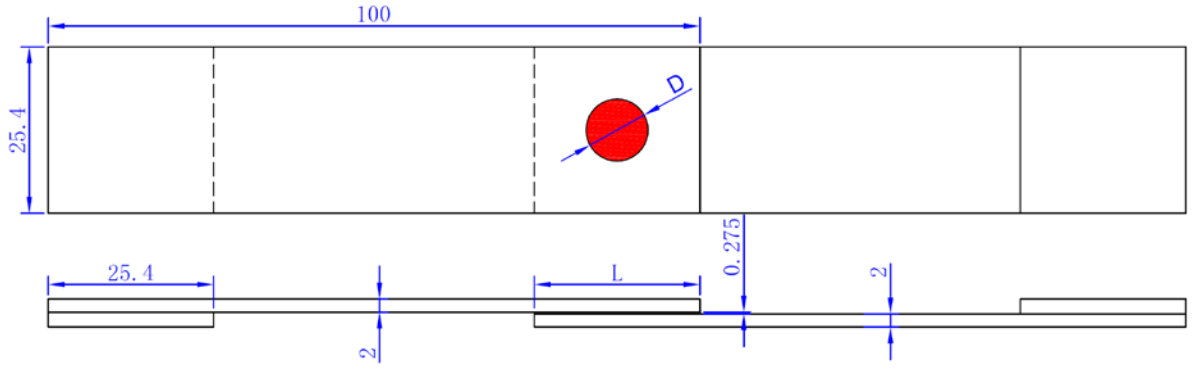
(b)

Fig.1. (a) Bulk adhesive specimen and (b) adhesive-bonded lap-shear joint configurations and dimensions (unit: mm).

Table 1. Adhesive-bonded lap-shear joint types.

| Joints	Type A	Type B	Type C	Type D	Type E	Type F
Bond line length, L (mm)	5.0	12.7	25.4	25.4	25.4	12.7
Tape diameter, D (mm)	0	0	0	8.0	20.0	0
Fillet	Arc	Arc	Arc	Arc	Arc	Full triangular

(a)

7

(b)

Fig.2. Schematics of (a) arc and (b) full triangular fillets.

Table 2. Mechanical properties of substrate and adhesive.

Materials	Young's Modulus (MPa)	Poisson's ratio	Yield strength (MPa)
AA6111-T4 (substrate)	70,000	0.33	224
BETAMATE 4601^{TM} (adhesive)	2,860	0.35	45

All tests were conducted on an MTS servo-hydraulic testing machine under ambient laboratory conditions (room temperature and atmospheric pressure), as shown in Fig.3. A clear plastic cover was used around the testing machine for protection. To eliminate the influence of mean stress, bulk adhesive specimens were tested under sinusoidal strain-controlled condition at a strain rate of 0.02/s and strain ratio R=-1. The extensometer gauge length is 12 mm. The glue was applied at the knife edges of the extensometer to prevent slipping. As for the lap-shear joints, both tensile shear strength and fatigue performance were evaluated. A displacement rate of 3 mm/min was adopted for the tensile tests. Fatigue tests were performed under load-controlled conditions at R=0.1. Constant sinusoidal waveforms at a frequency of 20 Hz were employed for all joints. The specimens were tested to failure or a maximum life of 15,000,000 cycles. The fatigue cycles were determined until the complete separation of joints.

8
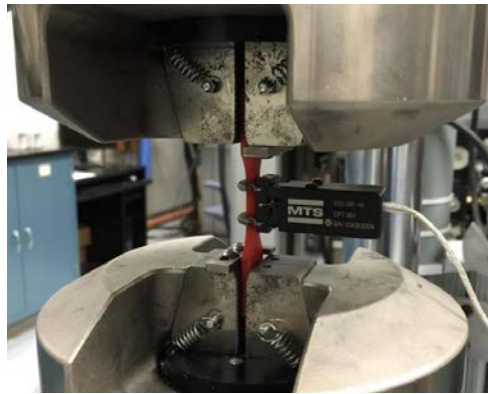
(a)

(b)

Fig.3. Setup of the tests on (a) bulk adhesive specimen and (b) adhesive-bonded lap-shear joint.

2.2 Lap-shear joints test results

To illuminate the effects of the adhesive fillet, overlap length, and un-bonded area, test data is presented against both applied load and tensile shear stress[28] (i.e., maximum tensile load divided by the overlap area). The comparison of the tensile shear strengths and critical tensile

9

shear stresses between all six types of joints is shown in Fig.4. The influences of the adhesive fillet, overlap length, and un-bonded area on fatigue failure life are illustrated in Fig.5. In terms of applied load, both the fillet and the overlap length have a positive influence on tensile shear strength and fatigue failure life of adhesive-bonded joints although the mechanisms differ. Furthermore, even with a similar bonded area, e.g., a 322.6 mm^2 for Type B and 331.0 mm^2 for Type E, the average tensile shear strength of Type B joint is still much lower than that of Type E joint, which indicates that the actual bonded area is not a quantifying indicator for the strength evaluation of adhesive-bonded joints under lap-shear loading condition. As for tensile shear stress, the effects of the un-bonded area and adhesive fillet can be found similar to those for applied load, but the overlap length works oppositely. One of the possible reasons is that although the tensile shear strength of the joints increases, the actual load-bearing area does not increase proportionally with the overlap area increasing, leading to the decrease of its proportion in the overlap area, and thus the critical tensile shear stress is lowered and fatigue failure life shortened.
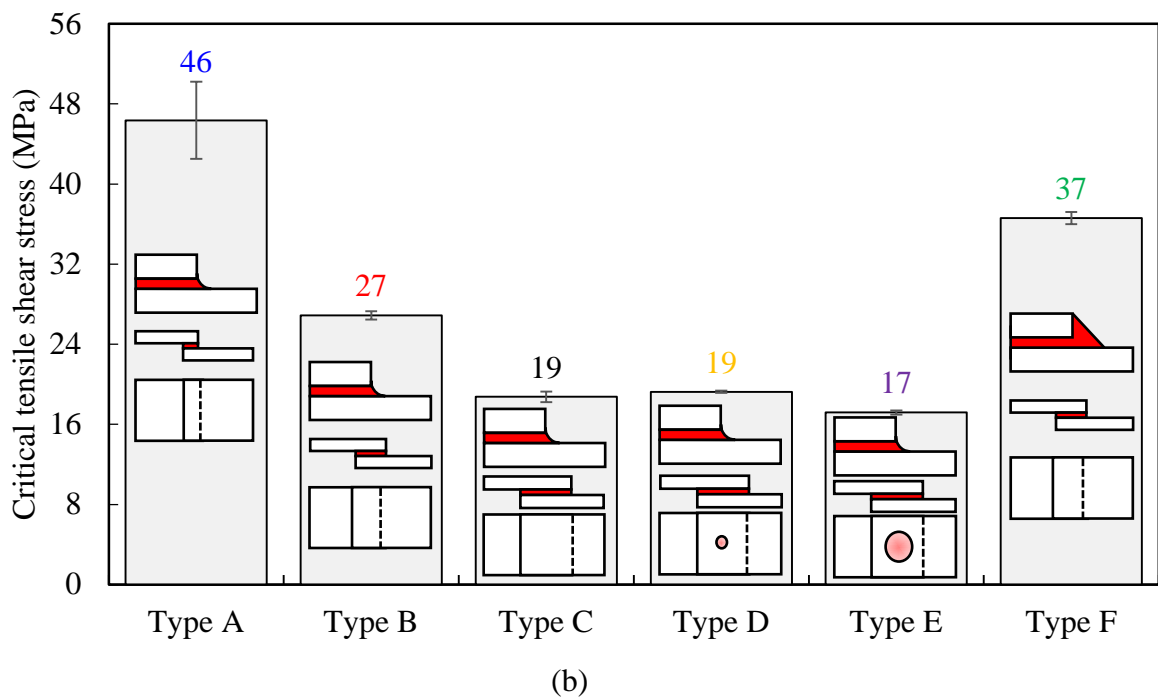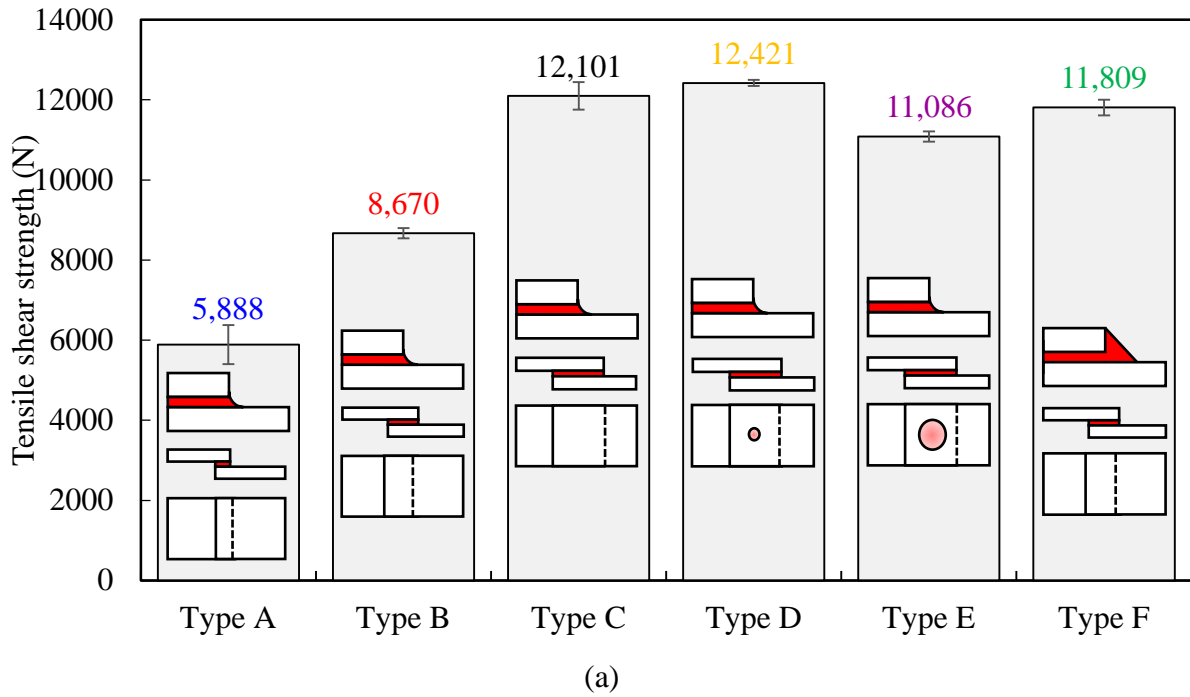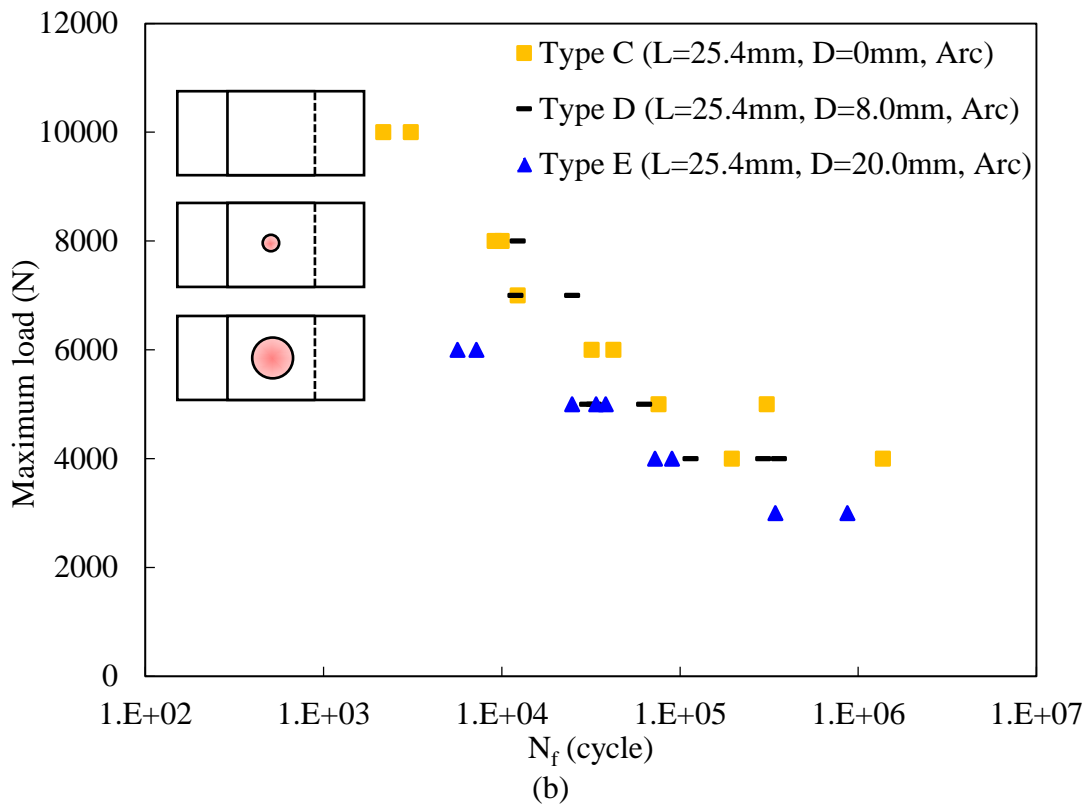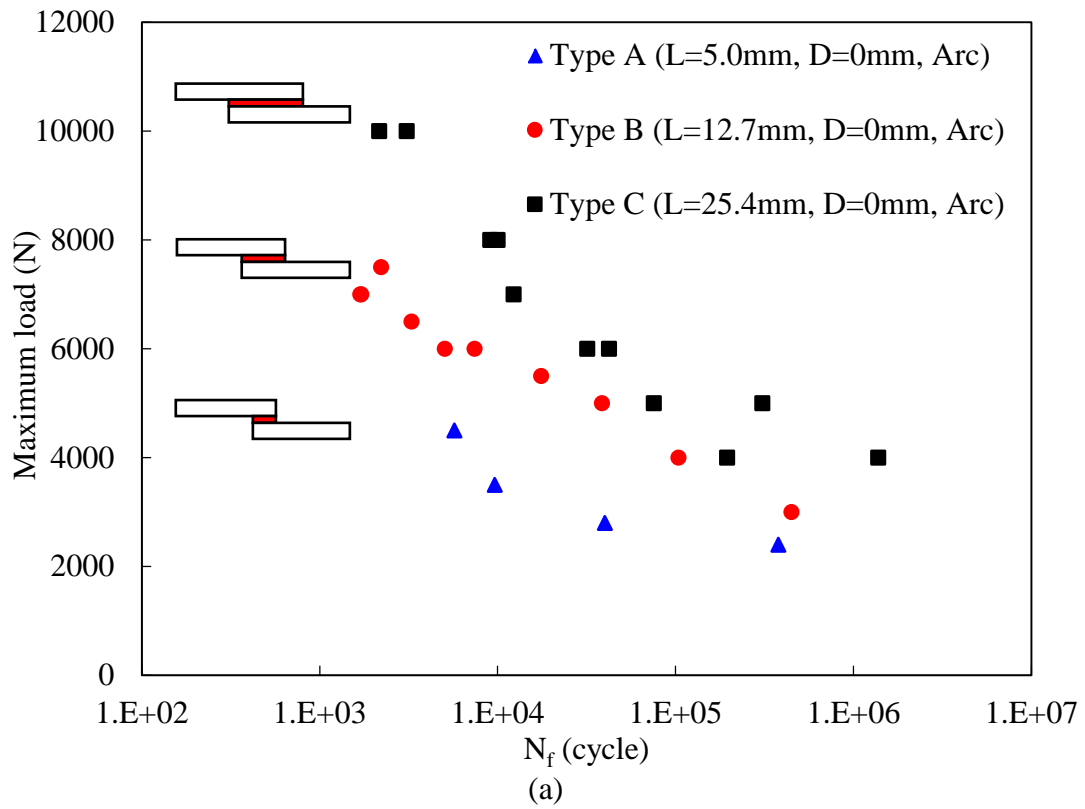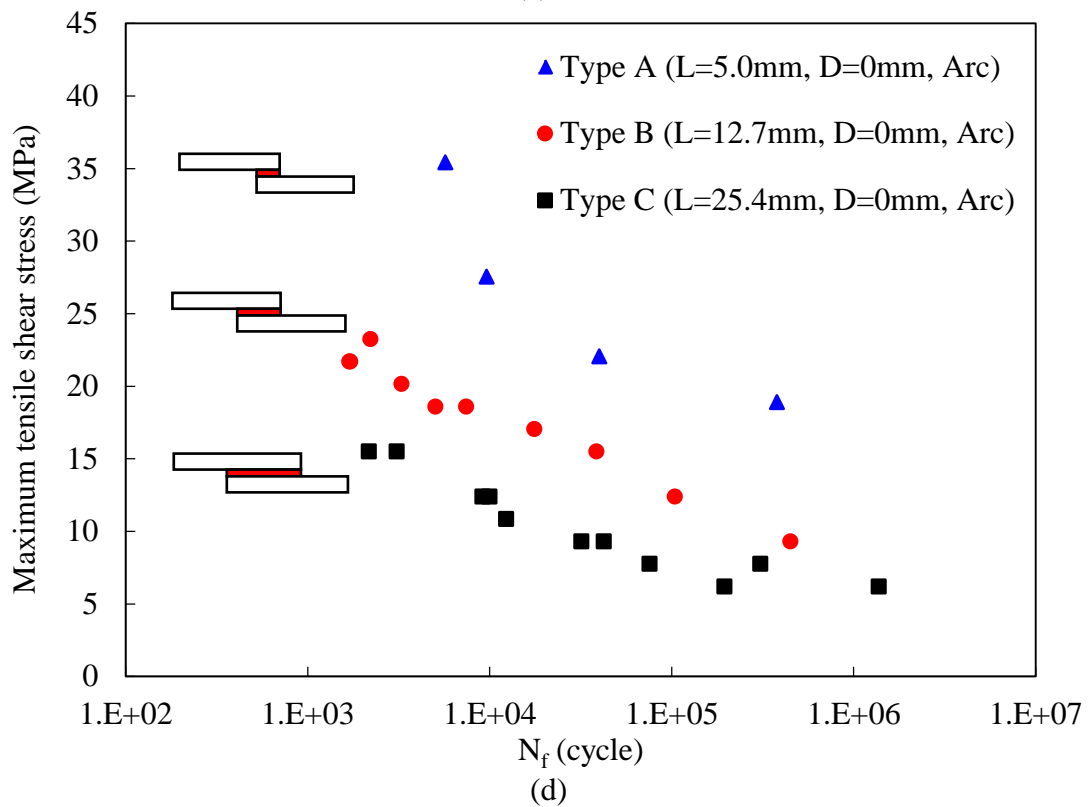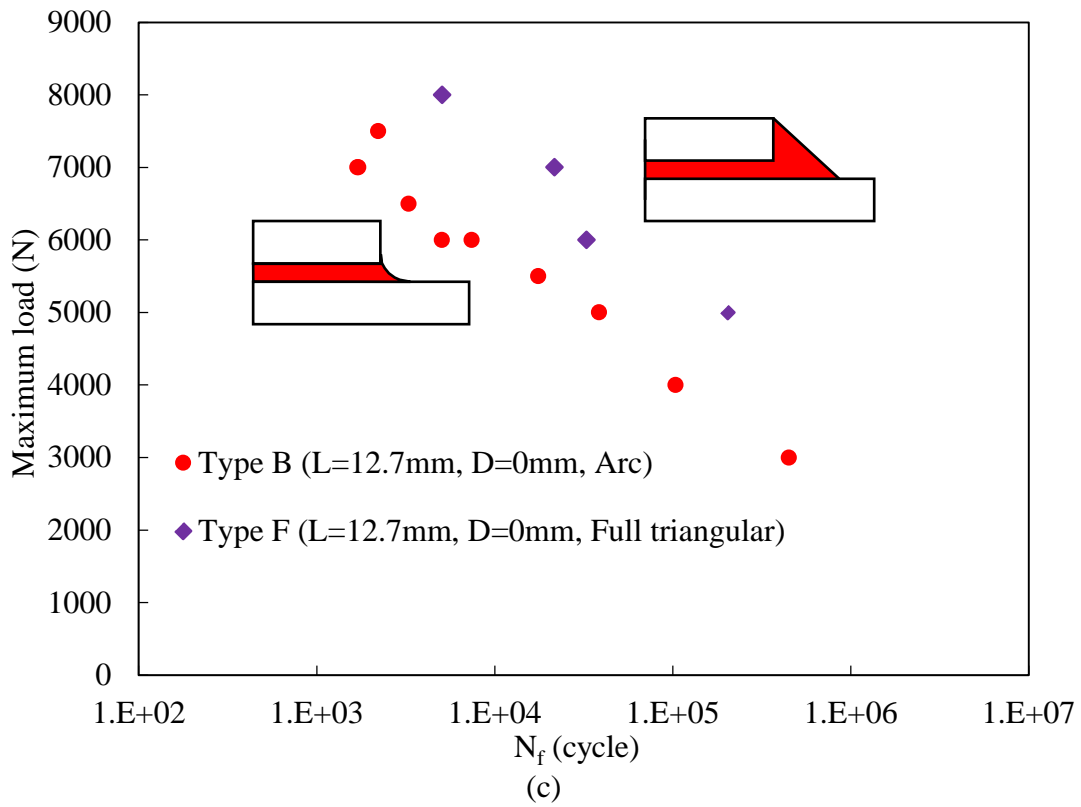
Fig.4. Comparison of (a) tensile shear strength and (b) critical tensile shear stress between lap-shear joints.

(a)

(b)
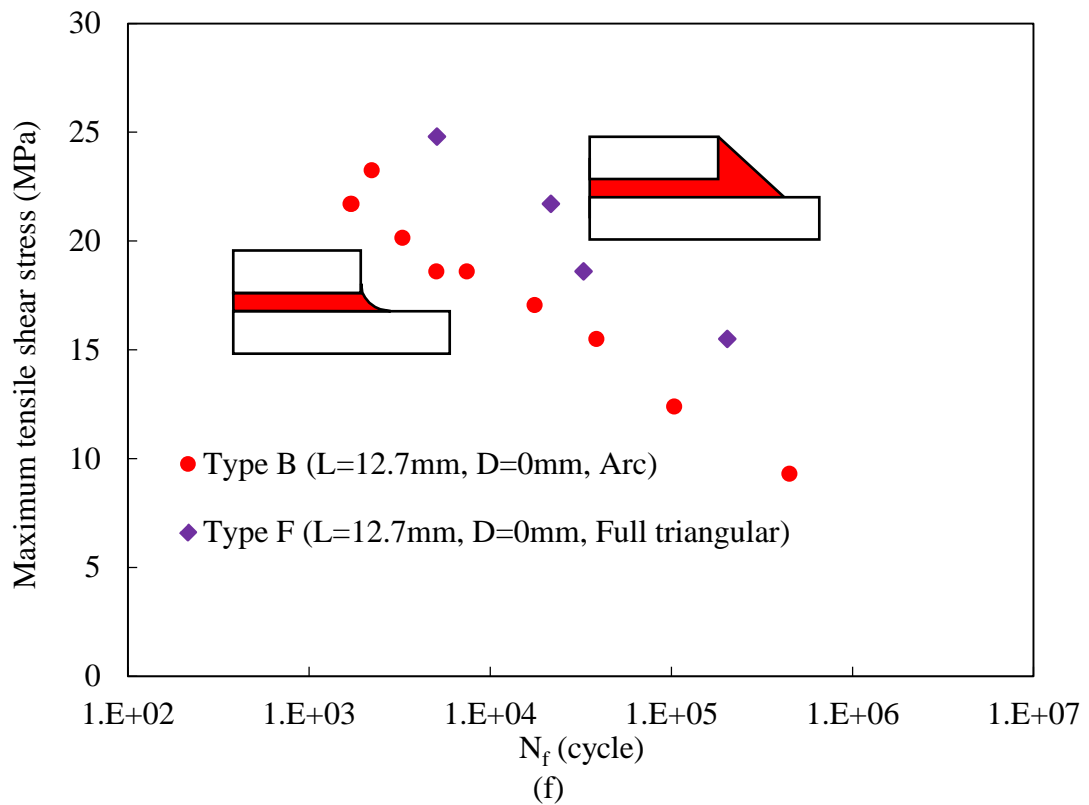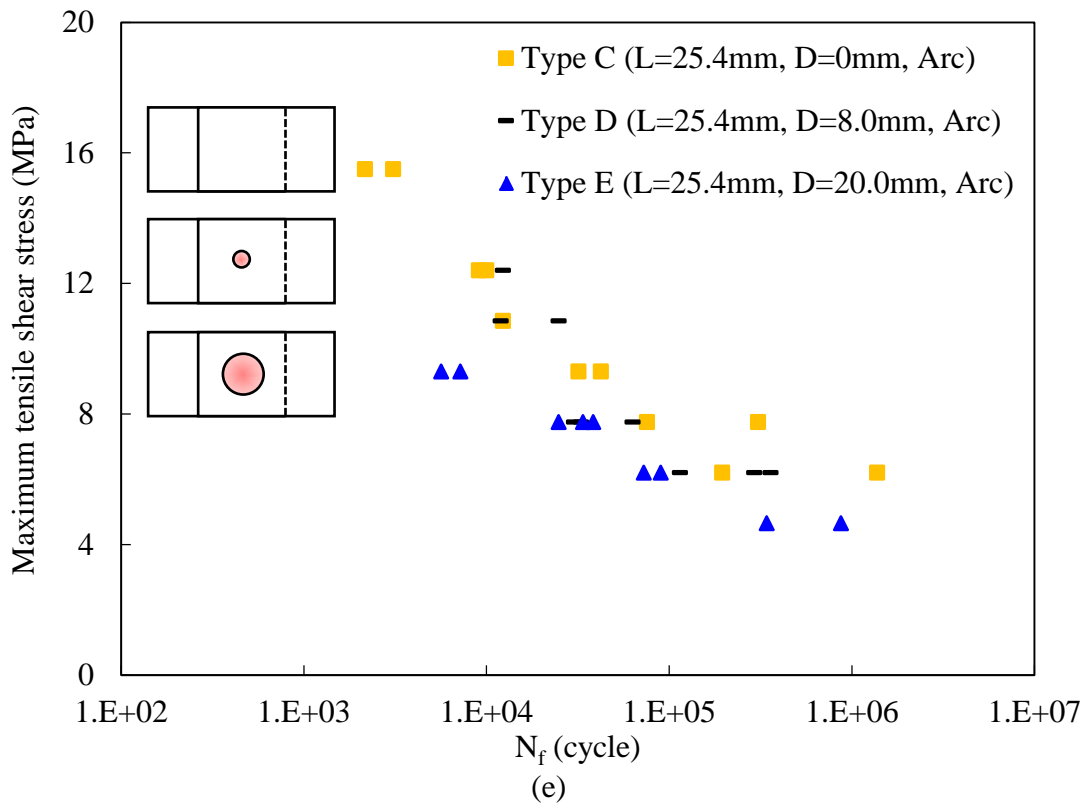
12

(c)

(d)

13

(e)

(f)

14

Fig.5. Comparison of fatigue failure lives between lap-shear joints on the effects of (a) overlap length, (b) un-bonded area, (c) adhesive fillet against applied load, and the effects of (d) overlap length, (e) un-bonded area, (f) adhesive fillet against tensile shear stress.

Fig.6 shows the typical fatigue crack path around the adhesive fillets and the dimensions of the local structure. As for an arc fillet, the crack initiation is at the outer edge of the fillet (red arrow shown in Fig.6a), consistent with the observation of Quaresimin and Ricotta[37]. For a full triangular fillet, the corner of the substrate (red arrow shown in Fig.6b) is considered as the crack initiation site based on the simulation results of O'Mahoney et al.[38] and the experimental results of Shenoy et al.[39].

(a)

15
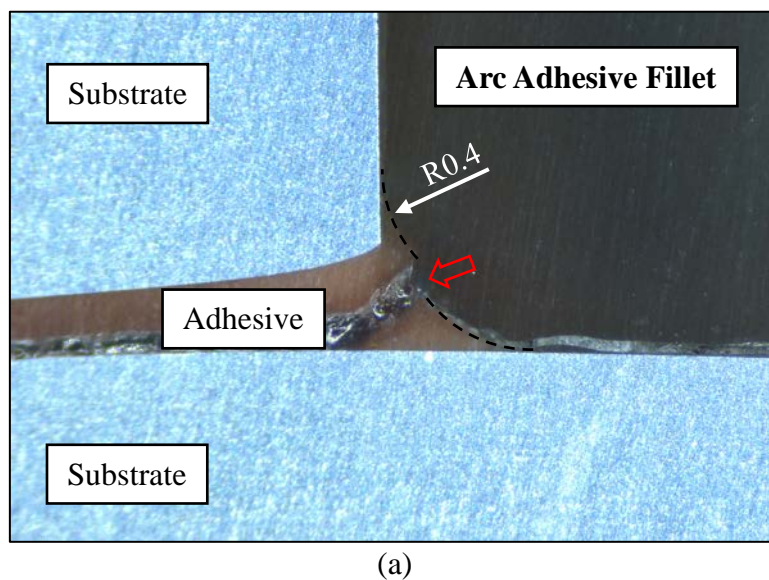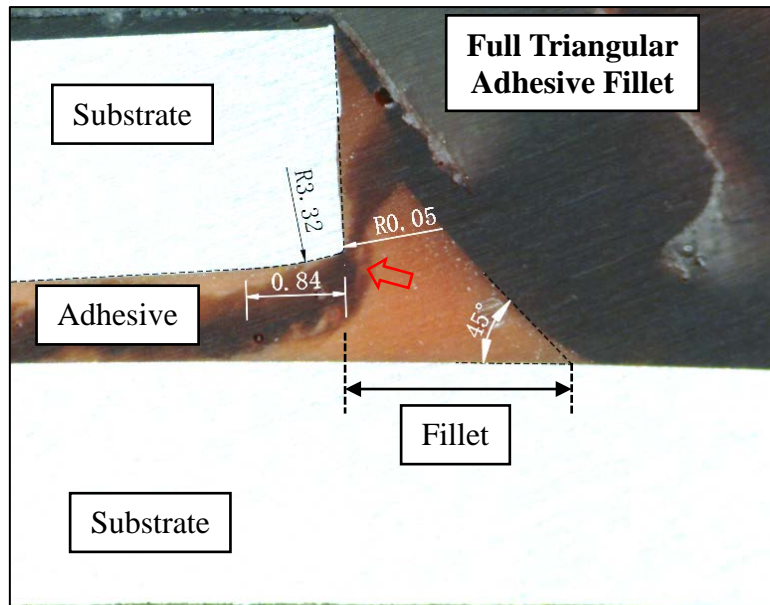
(b)

Fig.6. Fatigue crack path and local structure dimensions in (a) arc and (b) full triangular adhesive fillets (unit: mm). (Red arrows indicate the fatigue crack initiation sites.)

16

3. Total fatigue life evaluation

The total fatigue life of adhesive-bonded joint is calculated by adding the crack initiation life and crack growth life. Initiation life is calculated through a Manson-Coffin-Basquin equation which is fitted by using fatigue test data of bulk adhesive specimens. Detailed FE models of adhesive fillets are adopted to obtain the local strain in order to use this equation for initiation life calculation. Crack growth life is calculated by the integration of loading cycles on the crack growth path. Different crack growth paths are identified for different types of joints.

3.1 Crack initiation

The local strain-stress approach is adopted to estimate the fatigue failure location and crack initiation lives based on the widely used assumption[40] that life spent on crack nucleation of a notched component is identical to that of a smooth laboratory specimen under the same cyclic deformation.

3.1.1 Manson-Coffin-Basquin equation

To correlate the local strain to crack initiation, the strain-life curve of bulk adhesive specimens is described by the classic Manson-Coffin-Basquin equation, as listed in Eq.(1), shown in Fig.7 together with the test results.

$$\varepsilon_a = \frac{\sigma_f'}{E}(2N_i)^b + \varepsilon_f'(2N_i)^c \tag{1}$$

17

where ε_a is the strain amplitude, σ'_f and ε'_f respectively refer to the fatigue strength coefficient and fatigue ductile exponent, and superscripts b and c are the fatigue strength exponent and the fatigue ductile coefficient. All the parameters shown in Eq.(1) were obtained through curve fitting and are listed in Table 3.
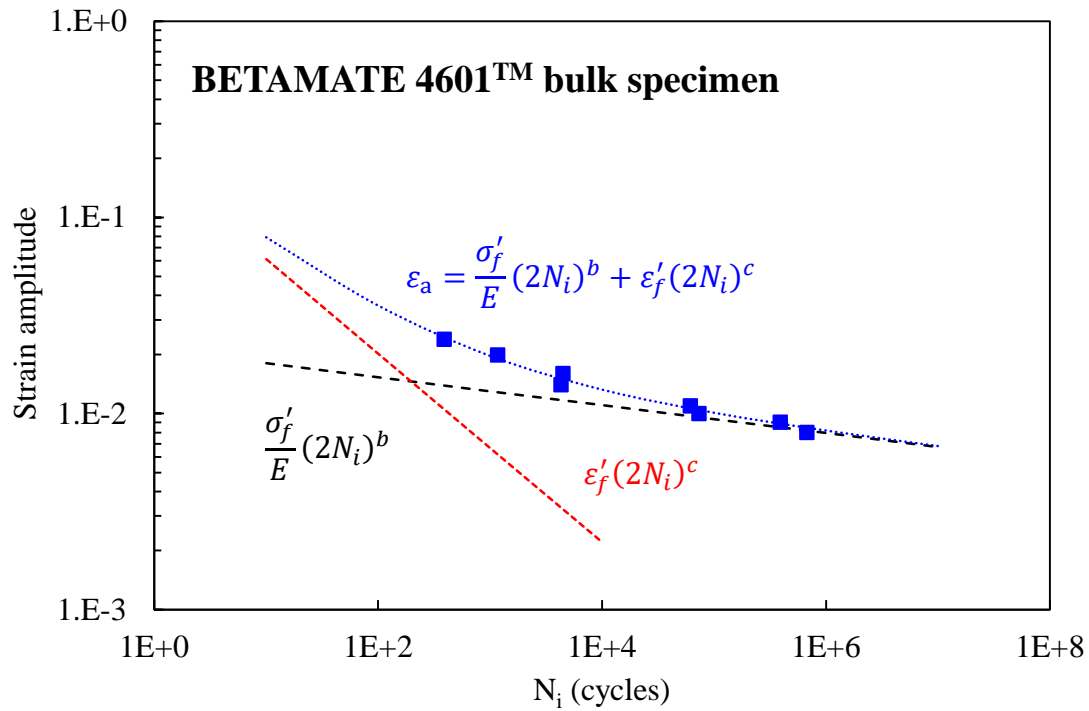

Fig.7. Strain-life curve of bulk adhesive specimens.

Table 3. Fatigue parameters in the Manson-Coffin-Basquin equation.

σ'_f (MPa)	ε'_f (MPa)	b	c	E (MPa)
63.807	0.25819	-0.07118	-0.48082	2,860

3.1.2 Finite element models

18

Full 3D finite element models are established by using ABAQUS^{TM}/standard to calculate the local maximum principal strain. Fig.8a and Fig.8b show the overviews of typical FE models of adhesive-bonded lap-shear joints with arc and full triangular fillets, respectively. An example of the un-bonded area in the models is shown in Fig.8c. Models were constructed with 20-node hex elements (C3D20) and refined at adhesive fillets with the element size of 5 μm, as shown in Fig.8d and Fig.8e. Fig.9 shows the uniaxial stress-strain curves of the substrate and adhesive used in the FE models.

(a)

19

(b)

Unbonded area

(c)

20
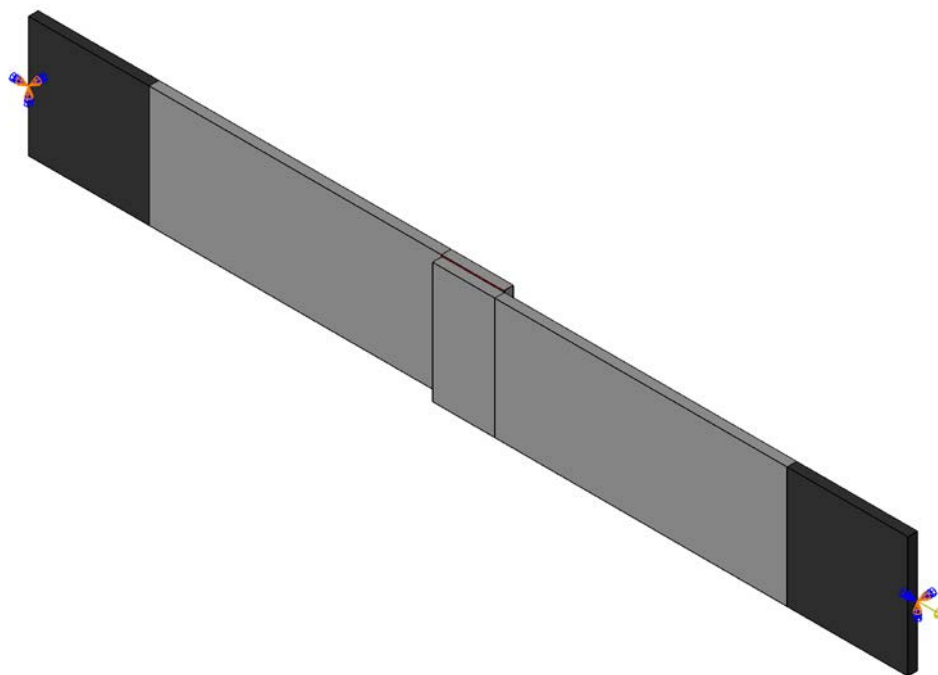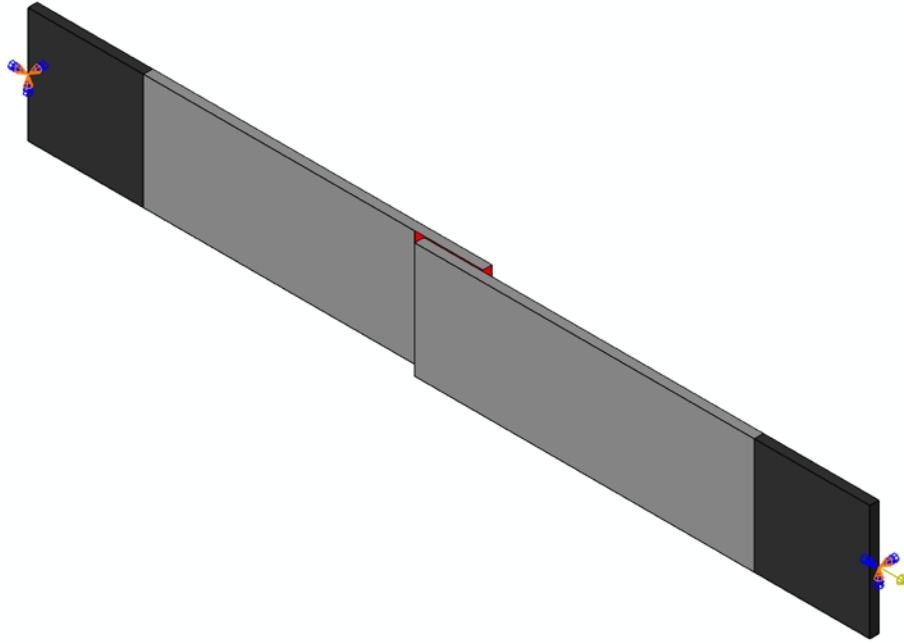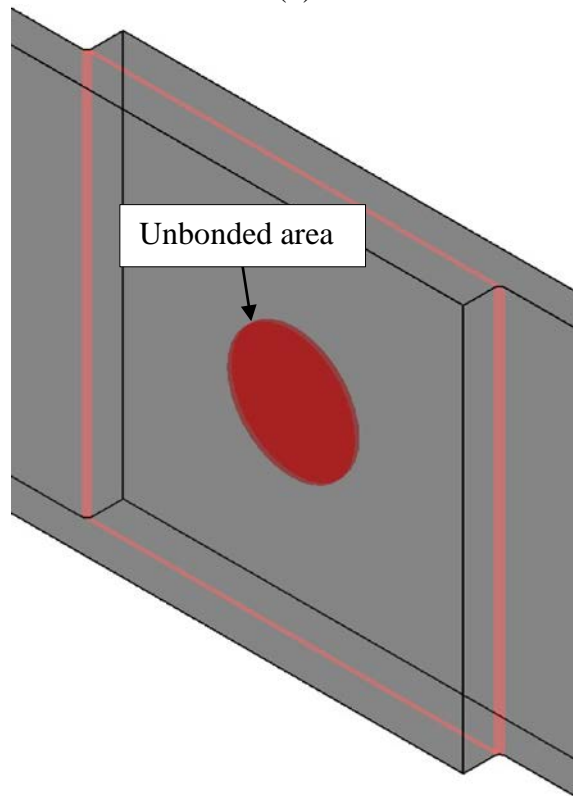
(d)

(e)

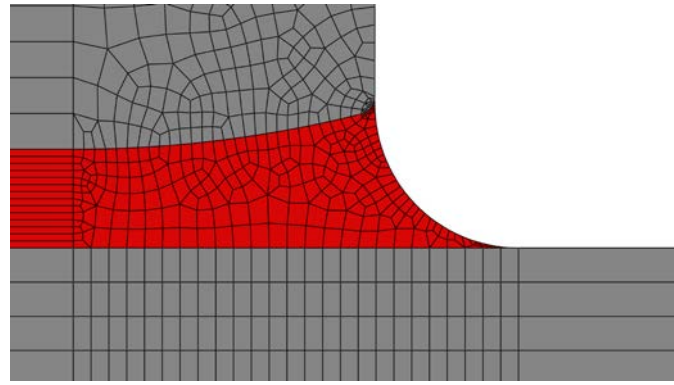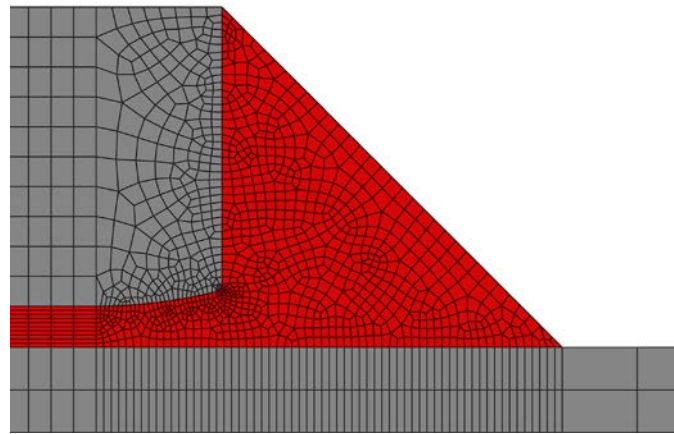Fig.8. (a) Overview of FE model with arc adhesive fillet, (b) overview of FE model with full triangular adhesive fillet, (c) un-bonded area in FE model, (d) local mesh in arc adhesive fillet and (e) local mesh in full triangular adhesive fillet.

.

21
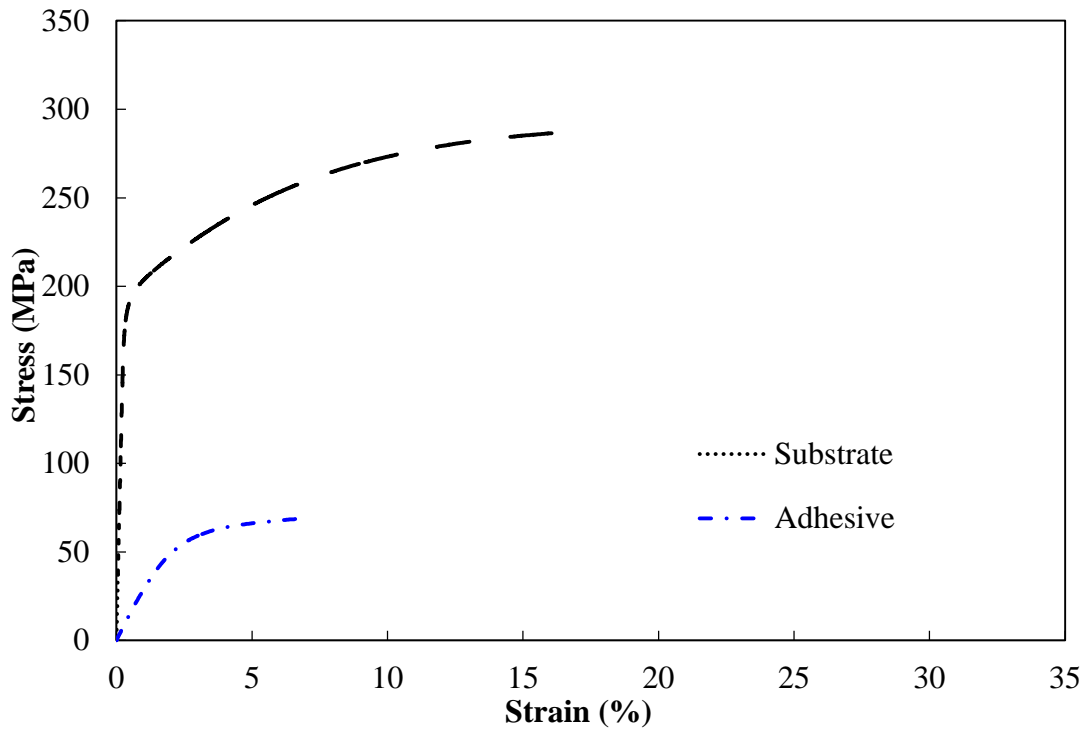
Fig.9. Uniaxial stress-strain curves for substrate and cured adhesive materials (reproduced from Ref.[41]).

Fig.10 shows the typical distributions of the maximum principal plastic strain on a symmetric plane in adhesive fillets at an external load of 4,000 N. As can be seen from the figures, the crack initiation occurs on the outward side of the fillet in an arc adhesive fillet and at the corner of the substrate for a full triangular adhesive fillet, consistent with experimental results shown in Fig.6. The maximum local principal strain at the crack initiation site will be used to calculate the initiation life through Eq.(1) and the calculated results will be presented in section 3.3.

22

(a)

(b)
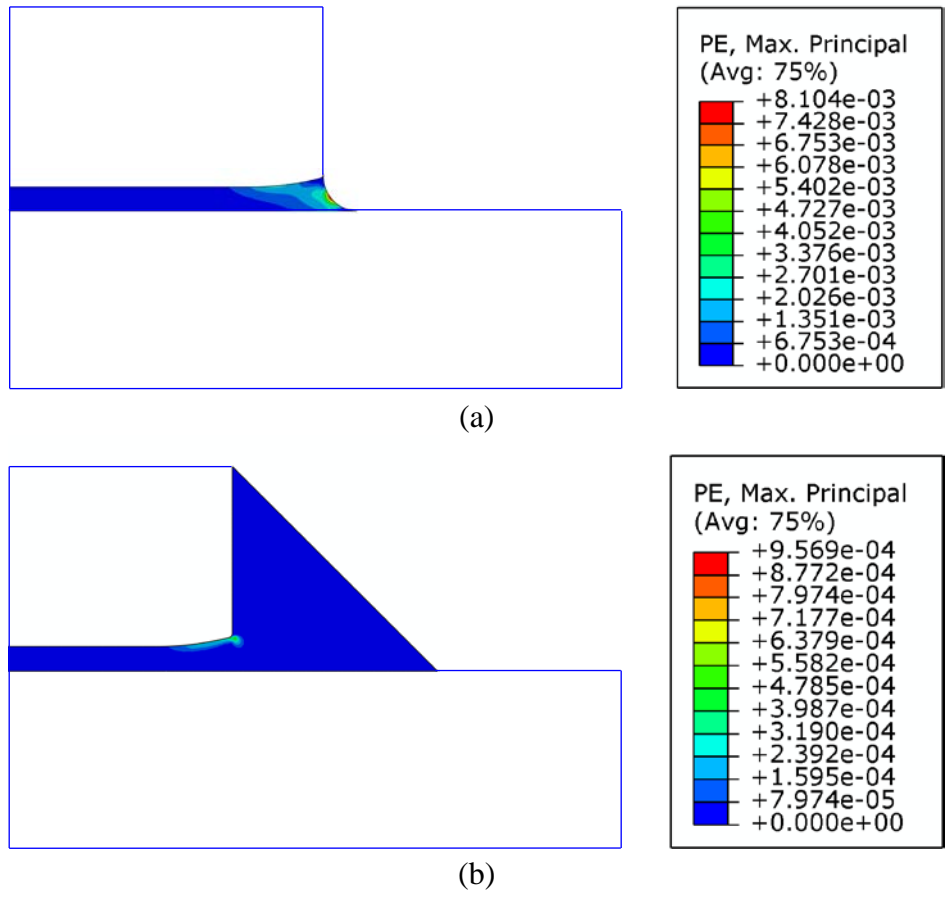
Fig. 10. Distribution of maximum principal plastic strain around adhesive fillets on the symmetric plane in (a) Type B and (b) Type F joints.

3.2 Mixed mode crack growth

Crack growth life is calculated by integrating crack growth rate equation in the form of strain energy release rates from initial crack length to final failure. To account for the mixed mode ratio effect, the interfacial crack model is incorporated into mixed mode crack growth to calculate the strain energy release rate for each mode.

3.2.1 Strain energy release rates

For simplification, the adhesive layer thickness is neglected due to the small ratio (6%) of bond line thickness to total stack-up thickness. Considering the significant effect of the mixed mode ratio on crack growth rates in an adhesive bonded system[30], the interfacial crack model[42,43] is employed to calculate the strain energy release rates for each mode. The schematic of the interfacial crack model is shown in Fig.11. The x-axis is defined to be along the direction from the center of the adhesive element perpendicularly to the edge of the adhesive layer, the y-axis follows the right-hand rule in $z \times x$, and z is the direction from the thicker substrate to the thinner one. t_l is the thickness of the substrates. F_l and M_l are the line force and line moment applied on the lth layer substrate in FE models (Fig.8), calculated through the structural load method[3]. l=1, 2 for the upper and lower debonded substrates, respectively, and l=3 for the joined side. Assume $t_1 \leq t_2$, without loss of generality.
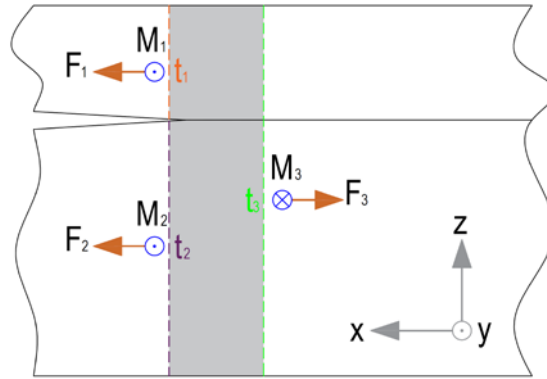
Fig. 11. Schematic of interfacial crack.

The structural loads that govern the crack tip singularity in Fig.11 can be calculated by superposition methods[42,43] and are as follows

$$F = \frac{1-\eta+\eta^2}{(1+\eta)^3} F_1 - \frac{(1-\eta+\eta^2)\eta}{(1+\eta)^3} F_2 - \frac{6\eta^2}{(1+\eta)^3}(M_1 + M_2)/t_1 \tag{2}$$

$$M = \frac{1+3\eta+3\eta^2}{(1+\eta)^3} M_1 - \frac{\eta^3}{(1+\eta)^3} M_2 - \frac{\eta^3}{2(1+\eta)^3} F_1 t_2 + \frac{\eta^3}{2(1+\eta)^3} F_2 t_1 \tag{3}$$

24

Stress intensity factors (SIFs) for the interfacial crack model in Fig. 11 were derived from Refs.[42,43] numerically by using the structural loads, and expressed as

$$K_{\mathrm{I}} = -\left[F\sqrt{\frac{1+4\eta+6\eta^2+3\eta^3}{2t_1}}\cos\alpha + M\sqrt{\frac{6(1+\eta^3)}{t_1{}^3}}\sin(\alpha+\gamma) \right] \tag{4}$$

$$K_{\mathrm{II}} = -\left[F\sqrt{\frac{1+4\eta+6\eta^2+3\eta^3}{2t_1}}\sin\alpha - M\sqrt{\frac{6(1+\eta^3)}{t_1{}^3}}\cos(\alpha+\gamma) \right] \tag{5}$$

where

$$\eta = t_1/t_2 \tag{6}$$

$$\alpha = 52.1° - 3°\eta \tag{7}$$

$$\sin\gamma = \frac{\sqrt{3}\eta^2(1+\eta)}{\sqrt{(1+4\eta+6\eta^2+3\eta^3)(1+\eta^3)}} \tag{8}$$

Correspondingly, the strain energy release rates for each mode can be obtained, as follows:

$$G_i = \frac{K_i{}^2}{E'} \tag{9}$$

$$E' = \frac{8E_1E_2}{E_2(\kappa_1+1)(\nu_1+1)+E_1(\kappa_2+1)(\nu_2+1)} \tag{10}$$

$$\kappa_l = \begin{cases} 3 - 4\nu_l\text{ , for plane strain} \\[2mm] \frac{3-\nu_l}{1+\nu_l},\text{ for plane stress} \end{cases} \tag{11}$$

where K_i ($i =$ I, II) is the ith Mode SIF; G_i ($i =$ I, II) is the mode i strain energy release rate calculated using K_i; ν_l and E_l are the Poisson's ratio and Young's modulus at the lth layer, respectively; and E' is the equivalent Young's modulus of the adhesive-bonded structure, substituted by that of the substrate listed in Table 2 for engineering purposes.

3.2.2 Mixed mode crack growth model

25

To characterize the mixed mode ratio, the shear mode ratio factor[30] β is calculated as follows and shown in Fig.12 for all kinds of joints.

$$\beta = 1 - \frac{G_{\mathrm{I}}}{G_{\mathrm{T}}} \tag{12}$$

$$G_{\mathrm{T}} = G_{\mathrm{I}} + G_{\mathrm{II}} \tag{13}$$

where G_{I} and G_{II} are the mode I and mode II strain energy release rates (N/m) in a loading cycle, respectively. G_{T} is the corresponding total strain energy release rate.

As can be seen from Fig.12, for the studied lap-shear joints, the mode I strain energy release rate takes about half of the total, and the shear mode ratio factor is uniquely controlled by overlap length. As the overlap length increases from Type A to Type C, the stiffness in overlap area increases and reduces the local bending, leading to a decrease in mode I and an increase in mode II strain energy release rates, which will lower the crack growth rate[30]. On the other hand, the shear mode ratio factor barely changes from Type C to Type E, which may be induced by the unique stress profile in adhesive-bonded lap-shear joints. Based on the stress analysis in Ref.[41], serious stress concentration occurs at the ends of the overlap area in lap-shear joints, and the stress in the central region can be negligible. Most of the applied load in adhesive bonding is carried at the end of the bonded area. The presence of defects in the center may alter the stress profile in lap-shear joints, but not remarkably, and the load transfer path can hardly be changed, leading to the insignificant variation of structural loads and shear mode ratio factor.
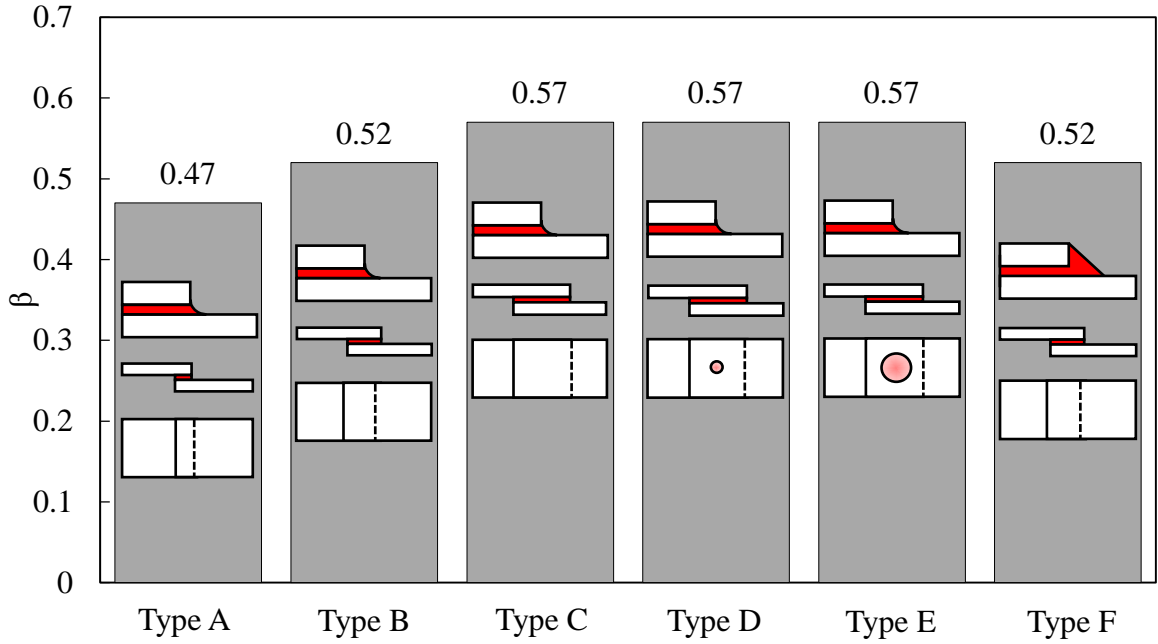
26

Fig.12. Shear mode ratio factor in different joints.

Based on our previous research[30], the fatigue performance of adhesive-bonded systems is dependent on loading mode mixity. To capture its effect, the mixed mode crack growth rate is expressed by a generalized Paris relation formula[30]:

$$\frac{da}{dN} = c(\beta) \cdot \left(pG_{\mathrm{I}}^2 + qG_{\mathrm{II}}^2\right)^{\frac{m(\beta)}{2}}, \ (\mathrm{mm/cycle}) \tag{14}$$

$$c(\beta) = (1 - \beta)c_1 + \beta c_2 \tag{15}$$

$$m(\beta) = (1 - \beta)m_1 + \beta m_2 \tag{16}$$

where $c(\beta)$ and $m(\beta)$ are the generalized coefficient and exponent, respectively. p, q, c_1, c_2, m_1, and m_2 are the material constants, which were obtained by fitting the crack growth rate data in our previous work[30], and listed in Table 4.

Table 4. Material constants[30] for fatigue crack growth in BETAMATE 4601[TM].

27

p	q	c_1	c_2	m_1	m_2
0.1816	0.0583	8.32e-12	1.43e-12	4.14	4.44

The crack growth life can be calculated by integrating the life cycles during crack growth. Based on the simulation results in Ref.[30], under shear-dominated loading, the SIFs increase as the crack growing, but not significantly. Thus, the initial strain energy release rates are adopted in the crack growth life calculation of lap-shear joints considering its insignificant variation during the crack evolution. The crack growth life can be derived as

$$N_p = \frac{a_f}{da/dN} \ (\text{cycle}) \tag{17}$$

where a_f is the final crack lengths used for different types of joints. Due to the symmetry, the cracks are treated equally at both loading sides of the studied lap-shear joints. Thus, the final crack lengths are calculated as half of the overlap length for fully bonded joints. For types D and E joints, the final crack length has to exclude the influence of the un-bonded area. Hence the final crack lengths are counted from the edge of adhesive to the nearest boundary of un-bonded area. Table 5 lists the calculated final crack lengths for different types of joints.

Table 5. Final crack lengths for different types of joints.

Final crack length	Type A	Type B	Type C	Type D	Type E	Type F
a_f (mm)	2.5	6.35	12.7	8.7	2.7	6.35

3.3 Results and discussion

28

Total fatigue failure life is calculated by adding initiation life (in Eq.(1)) and growth life (in Eq.(17)). Fig.13 compares the calculated total life with the experimental results. Good correlation between calculation and experimental results is achieved, and most of the data lie within 5-times of error band.
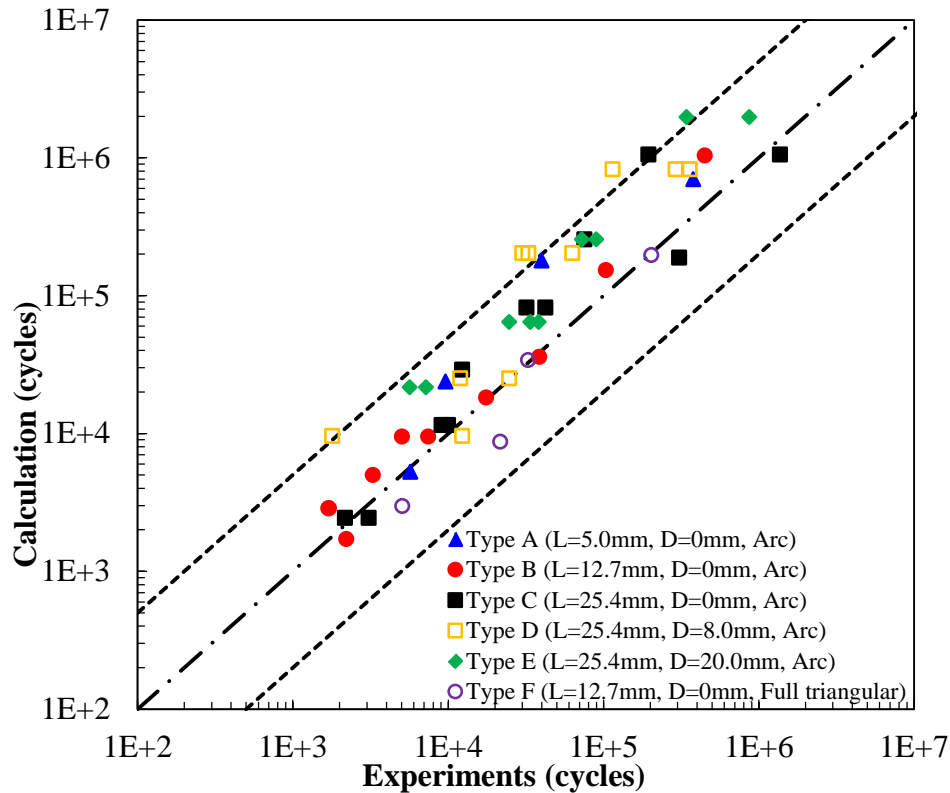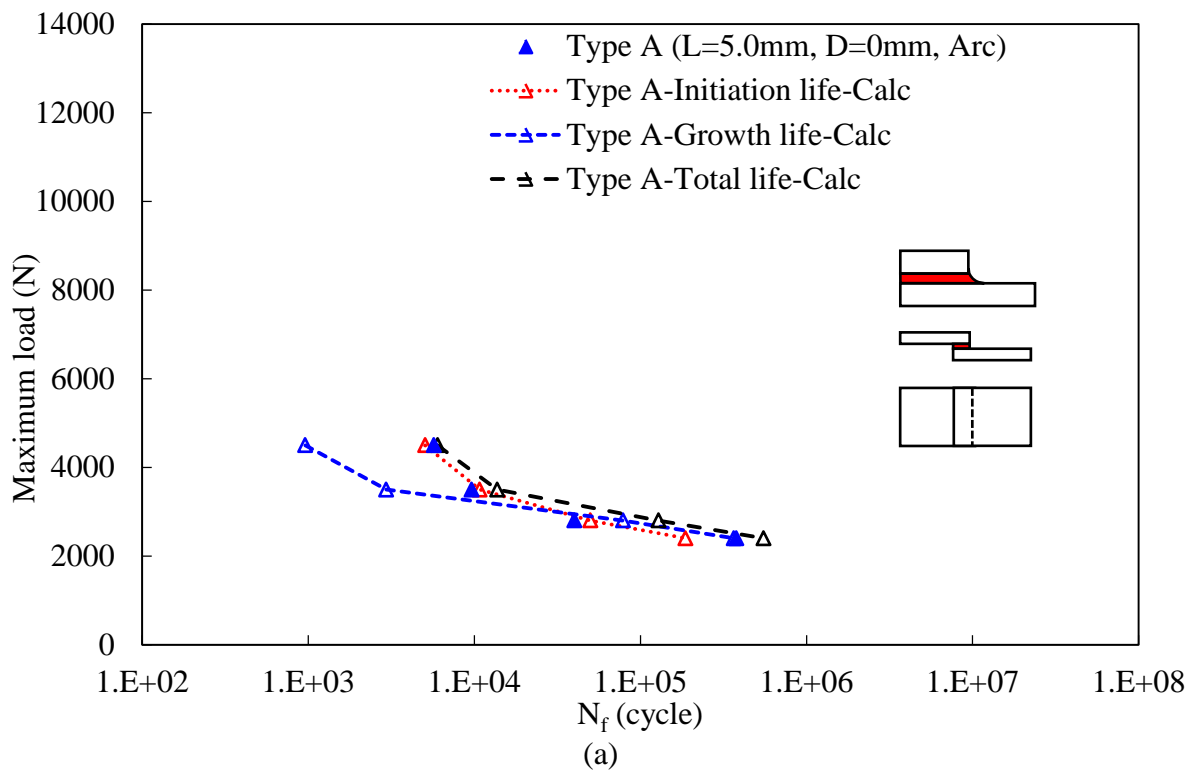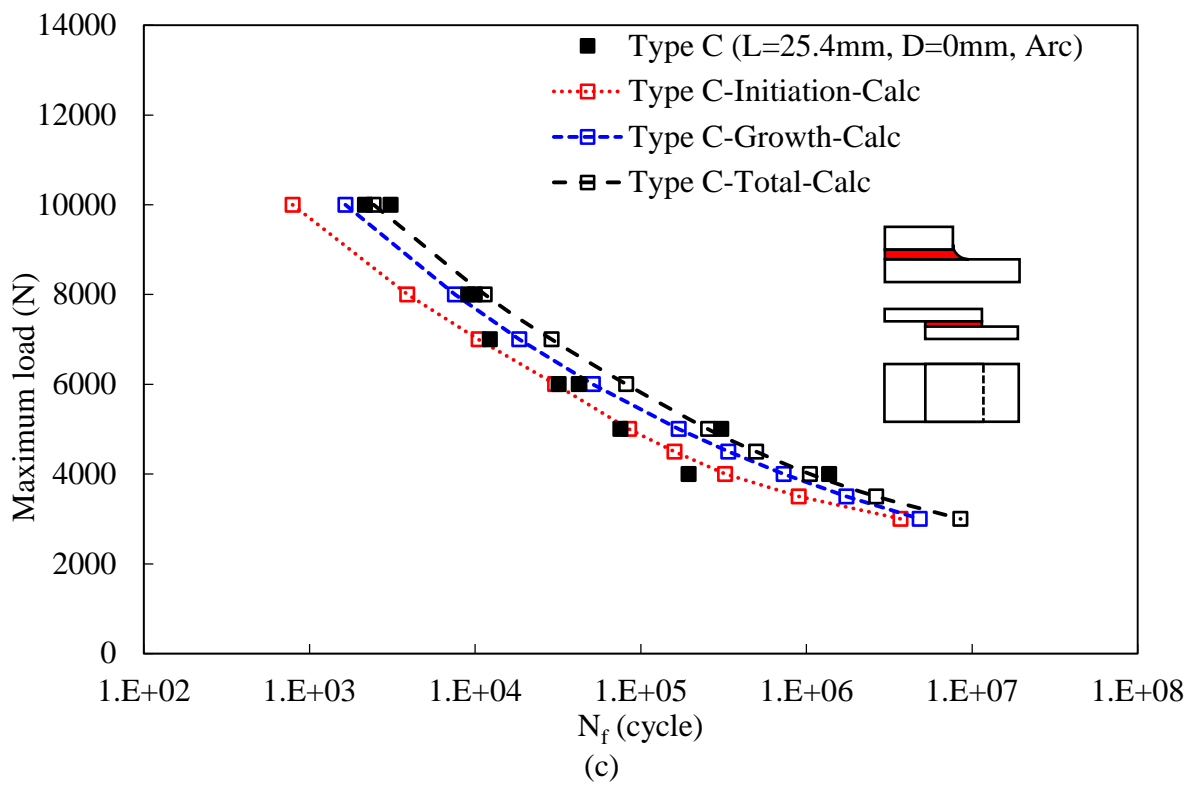

Fig.13. Comparison between calculation results and experiments.

Fig.14 compares the experimental and calculated results for all types of studied joints by separating the total fatigue life into crack initiation life and growth life. By comparing Fig.14a~c, the crack initiation life is dominant only for the overlap length of 5.0 mm (Type A). As for the overlap length of 12.7mm (Type B) and 25.4mm (Type C), the crack growth life is dominant. With the overlap length increasing, the shear mode ratio factor (Fig.12)

29

increases and the fraction of mode II strain energy release rate range (Eq.(12)) increases, slowing down the crack growth. The increased overlap length also prolongs the growth life by growing length. Fig.14c~e compare the results from Type C to Type E joints. It shows that the un-bonded area within the adhesive layer has a similar effect as overlap length. Increasing the un-bonded area decreases the crack growth life due to the shorter crack growth length, which explains why fatigue failure life of weld-bonded joints is smaller than that of similar adhesive-bonded joints[16]. However, the initiation life remains similar in three kinds of joints, indicating the insignificant effect of un-bonded area on crack nucleation. Fig.14b and Fig.14f compare the results of Type B and Type F joints. It shows that with the same crack growth length and growth life, the full triangular adhesive fillet significantly enhances the crack initiation life, leading to the increasing fatigue failure life of the joints.
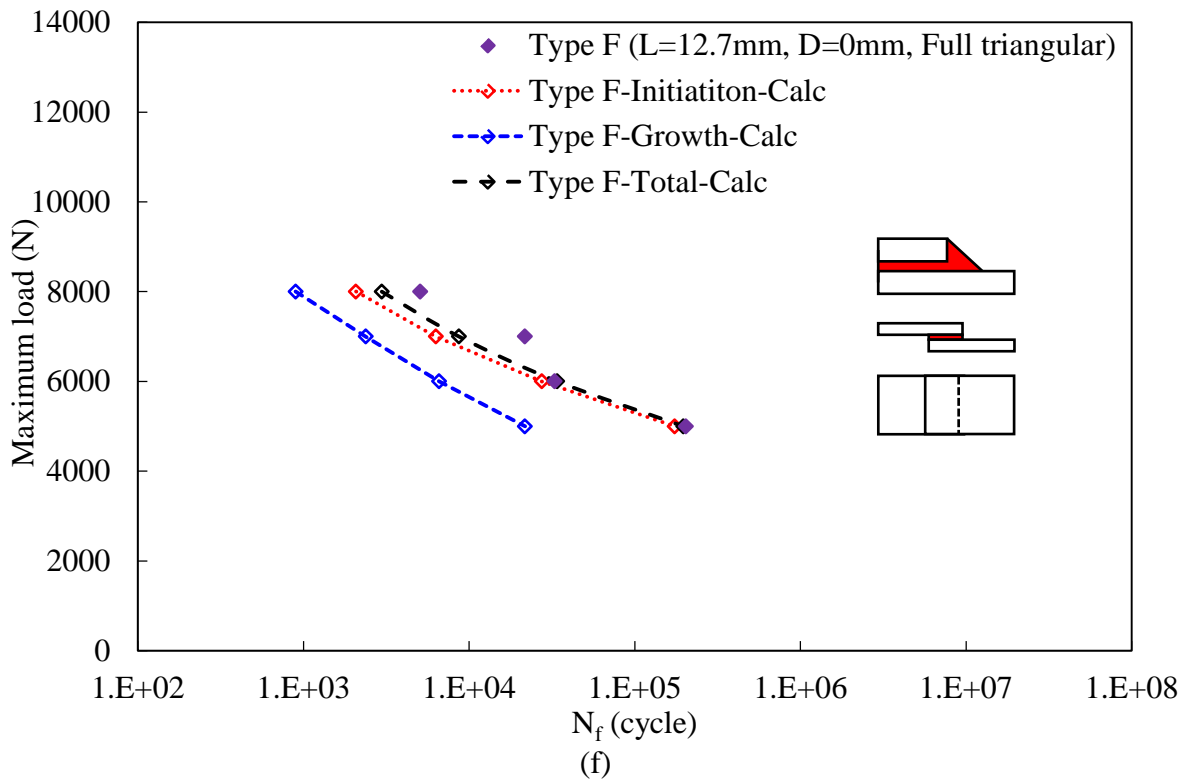

(a)

30

(b)

(c)

31

(d)

(e)

32
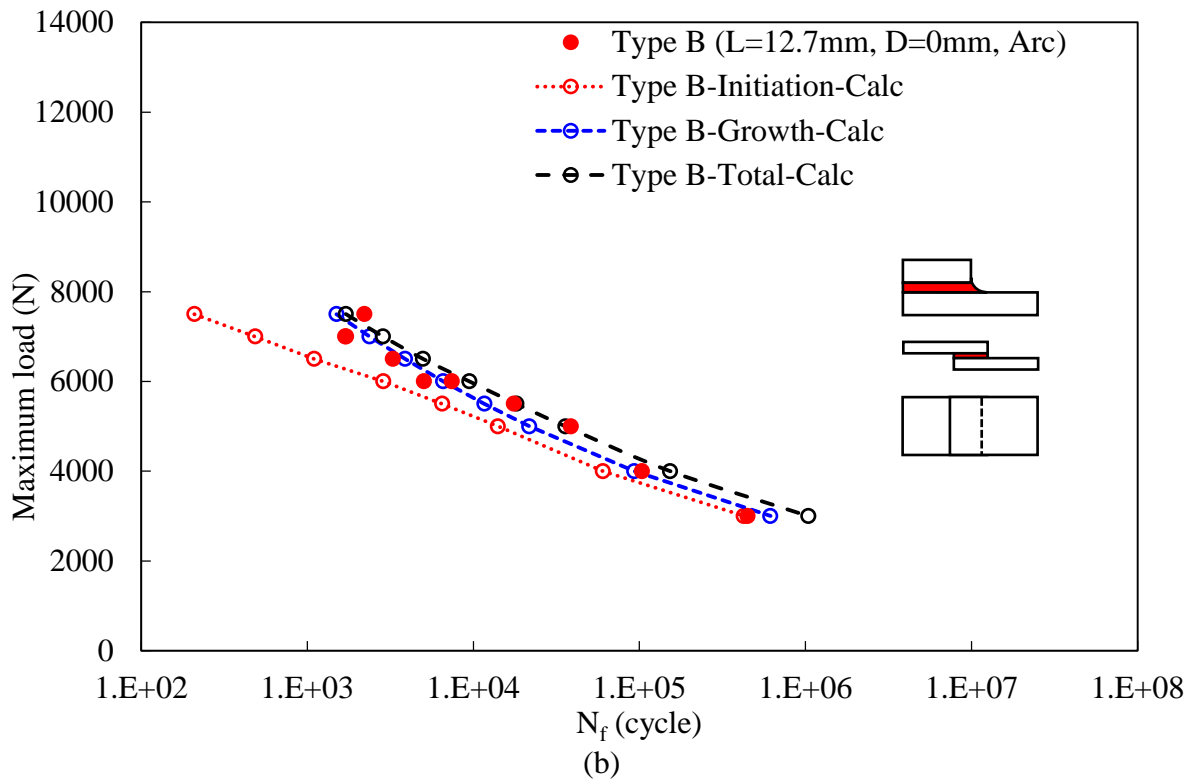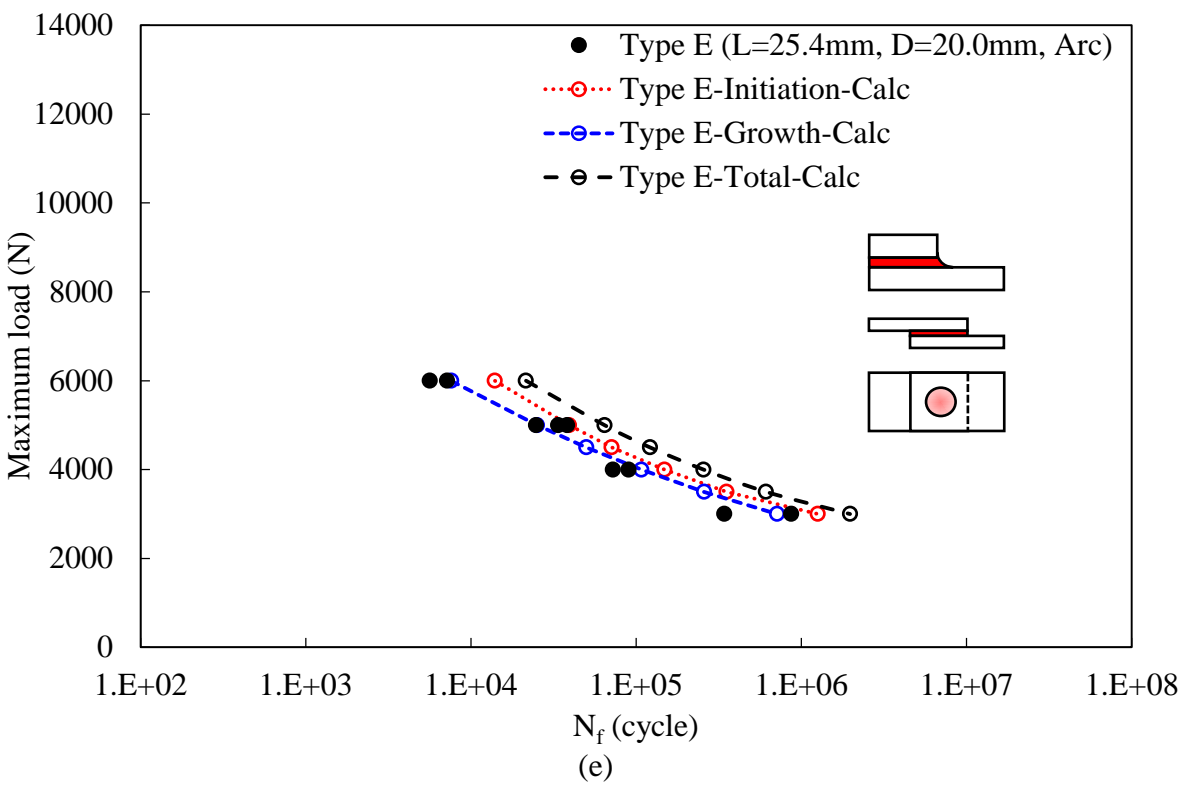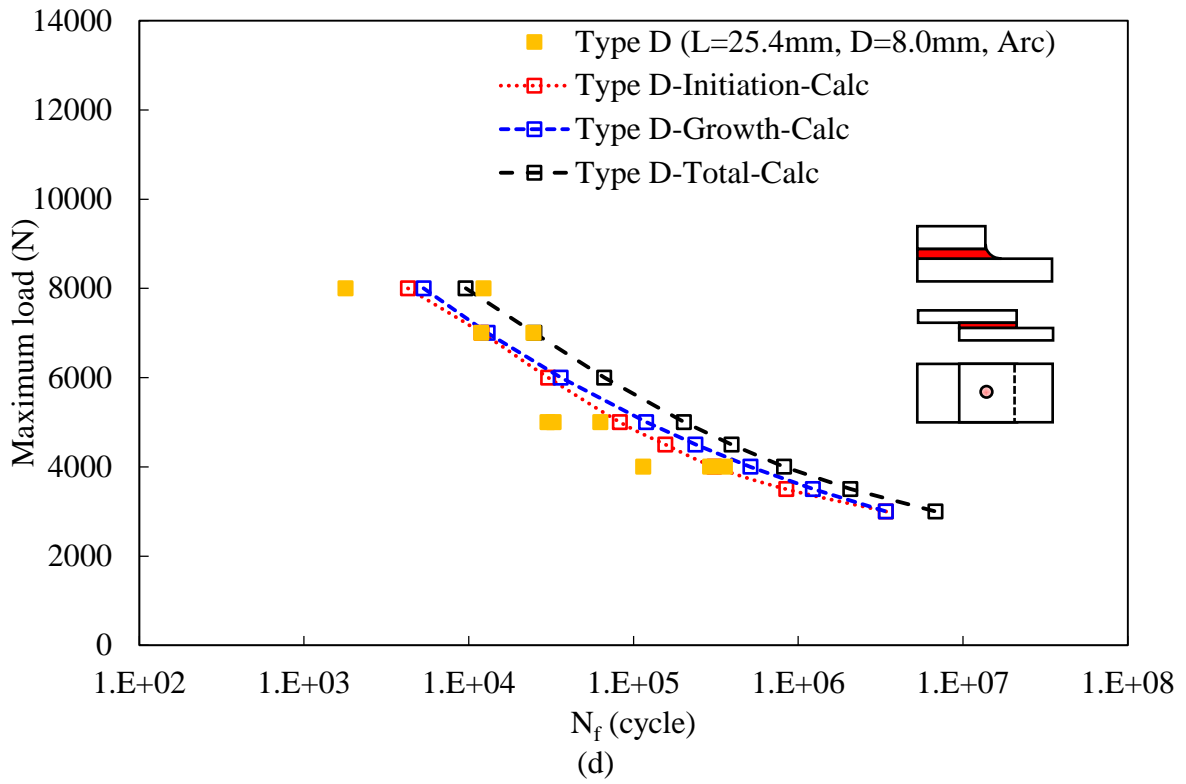
Fig. 14. Comparison between test results and calculated initiation life, growth life, and the total life in (a) Type A, (b) Type B, (c) Type C, (d) Type D, (e) Type E, and (f) Type F joints.

4. Conclusions

In this work, the effects of the adhesive fillet, overlap length, and un-bonded area of adhesive-bonded lap-shear joints are experimentally and numerically evaluated. A straightforward total fatigue life calculation method is proposed based on the local strain-stress approach and mixed mode crack growth method. The following conclusions can be drawn:

1. Both the adhesive fillet and the overlap length have a positive influence on the tensile shear strength of adhesive-bonded joints, while the un-bonded area has a negative impact.

2. By characterizing the initiation life with the local strain-stress approach, the crack initiation life and site are calculated based on detailed FE models. Crack initiation occurs at the outer edge of the arc adhesive fillet and the corner of the substrate edge in a full triangular adhesive fillet.

3. Crack growth life is calculated using the mixed mode crack growth method. An interfacial crack model and a generalized Paris relation formula are utilized to consider the effect of loading mode mixity. Final crack growth length is taken as half of the overlap length for fully bonded joints minus the radius of un-bonded area to account for its influence.

4. The entire fatigue failure life of adhesive-bonded joints is calculated by adding up crack initiation and growth lives. A good correlation between the calculated and the experimental results is obtained.

5. Although both larger adhesive fillet and overlap length enhance the fatigue failure life of adhesive-bonded joints, the mechanisms are completely different. A full triangular adhesive

34

fillet significantly postpones the crack initiation through a lower local strain level. The overlap length increases the crack growth life by enhancing the crack growth length and the fraction of mode II strain energy release rate, which leads to lower crack growth rate.

6. The un-bonded area also decreases the crack growth length. Nevertheless, due to the relatively large fraction of the crack initiation life, the effect of the un-bonded area on fatigue performance is relatively insignificant.

35

Acknowledgements

36

References

1. Vantadori S, Ronchei Camilla, Carpinteri A. Multiaxial fatigue life evaluation of notched structural components: An analytical approach. *Material Design & Processing Communications*, 2019;1(4): e74.

2. Ghosh PK, Avantak P, Kaushal K. Adhesive joining of copper using nano-filler composite adhesive. *Polymer*, 2016; 87: 159–169.

3. Chen Q, Guo H, Avery K, Su X, Kang H. Fatigue performance and life estimation of automotive adhesive joints using a fracture mechanics approach. *Engineering Fracture Mechanics*, 2017; 172: 73–89.

4. Lißner M, Alabort E, Cui H, Pellegrino A, Petrinic N. On the rate dependent behaviour of epoxy adhesive joints: Experimental characterisation and modelling of mode I failure. *Composite Structures*, 2018; 189: 286–303.

5. De Moura MFSF, Gonçalves JPM, Silva FGA. A new energy based mixed-mode cohesive zone model. *International Journal of Solids and Structures*, 2016; 102: 112–119.

6. Weißgraeber P, Becker W. Finite fracture mechanics model for mixed mode fracture in adhesive joints. *International Journal of Solids and Structures*, 2013; 50(14 –15): 2383–2394.

7. Han X, Akhmet G, Zhang W, Chao YX, Jin Y, Yu Y, Hu P, Ibraimov A. The effect of adhesive fillet on mechanical performance of adhesively bonded corrugated sandwich structures: an experimental–numerical study. *The Journal of Adhesion*, 2020; 96(5): 515–537.

37

8. Zielecki W, Kubit A, Kluz R, Trzepieciński T. Investigating the influence of the chamfer and fillet on the high-cyclic fatigue strength of adhesive joints of steel parts. *Journal of Adhesion Science and Technology*, 2017; 31(6), 627–644.

9. Solana AG, Crocombe AD, Wahab MA, Ashcroft IA. Fatigue initiation in adhesively-bonded single-lap joints. *Journal of Adhesion Science and Technology*, 2007; 21(14), 1343–1357.

10. Abdel Wahab MM. Fatigue in adhesively bonded joints: a review. *ISRN Materials Science*, 2012.

11. Azari S, Papini M, Schroeder JA, Spelt JK. Fatigue threshold behavior of adhesive joints. *International Journal of Adhesion and Adhesives*, 2010; 30(3), 145–159.

12. Sugiman S, Crocombe AD. The static and fatigue responses of aged metal laminate doublers joints under tension loading. *Journal of Adhesion Science and Technology*, 2016; 30(3), 313–327.

13. Kumar S, Pandey PC. Fatigue life prediction of adhesively bonded single lap joints. *International Journal of Adhesion and Adhesives*, 2011; 31(1), 43–47.

14. Miyazaki T, Noda NA. Evaluation of debonding strength of single lap joint by the intensity of singular stress field. In *Journal of Physics: Conference Series* (Vol. 842, No. 1, p. 012078). IOP Publishing, 2017, May.

15. Pashah S, Arif AFM. Fatigue life prediction of adhesive joint in heat sink using Monte Carlo method. *International Journal of Adhesion and Adhesives*, 2014; 50, 164–175.

16. Shahani AR, Pourhosseini SM. The effect of adherent thickness on fatigue life of adhesively bonded joints. *Fatigue & Fracture of Engineering Materials & Structures*, 2019; 42(2), 561–571.

17. Blaysat B, Hoefnagels JP, Lubineau G, Alfano M, Geers MG. Interface debonding characterization by image correlation integrated with double cantilever beam kinematics. *International Journal of Solids and Structures*, 2015; 55: 79–91.

18. Kim HB, Naito K, Oguma H. Fatigue crack growth properties of a two-part acrylic-based adhesive in an adhesive bonded joint: Double cantilever-beam tests under Mode I loading. *International Journal of Fatigue*, 2017; 98: 286–295.

19. Al-Khudairi O, Hadavinia H, Waggott A, Lewis E, Little C. Characterising mode I/mode II fatigue delamination growth in unidirectional fibre reinforced polymer laminates. *Materials & Design (1980–2015)*, 2015; 66: 93–102.

20. Wahab MA, Ashcroft IA, Crocombe AD, Smith PA. Finite element prediction of fatigue crack propagation lifetime in composite bonded joints. *Composites Part A: Applied Science and Manufacturing*, 2004; 35(2): 213–222.

21. Monteiro J, Akhavan-Safar A, Carbas R, Marques E, Goyal R, El-zein M, da Silva. Influence of mode mixity and loading conditions on the fatigue crack growth behaviour of an epoxy adhesive. *Fatigue & Fracture of Engineering Materials & Structures*, 2020; 43(2): 308–316.

22. Ayatollahi MR, Samari M, Razavi SMJ, da Silva LFM. Fatigue performance of adhesively bonded single lap joints with non-flat sinusoid interfaces. *Fatigue & Fracture of Engineering Materials & Structures*, 2017; 40(9): 1355–1363.

23. Solana AG, Crocombe AD, Ashcroft IA. Fatigue life and backface strain predictions in adhesively bonded joints. *International Journal of Adhesion and Adhesives*, 2010; 30(1): 36–42.

24. Shenoy V, Ashcroft IA, Critchlow GW, Crocombe AD. Unified methodology for the prediction of the fatigue behaviour of adhesively bonded joints. *International Journal of Fatigue*, 2010; 32(8): 1278–1288.

25. Tang JH, Sridhar I, Srikanth N. Static and fatigue failure analysis of adhesively bonded thick composite single lap joints. *Composites Science and Technology*, 2013; 86, 18–25.

26. Jen YM, Ko CW. Evaluation of fatigue life of adhesively bonded aluminum single-lap joints using interfacial parameters. *International Journal of Fatigue*, 2010; 32(2), 330–340.

27. Braga DF, Maciel R, Bergmann L, da Silva LF, Infante V, dos Santos JF, Moreira PM. Fatigue performance of hybrid overlap friction stir welding and adhesive bonding of an Al-Mg-Cu alloy. *Fatigue & Fracture of Engineering Materials & Structures*, 2019; 42(6): 1262–1270.

28. Xu W, Liu L, Zhou Y, Mori H, Chen DL. Tensile and fatigue properties of weld-bonded and adhesive-bonded magnesium alloy joints. *Materials Science and Engineering: A*, 2013; 563, 125–132.

29. Abdel Wahab MM, Hilmy I, Ashcroft IA, Crocombe AD. Evaluation of fatigue damage in adhesive bonding: part 2: single lap joint. *Journal of Adhesion Science and Technology*, 2010; 24(2): 325–345.

30. Chen Q, Guo H, Avery K, Kang H, Su X. Mixed-mode fatigue crack growth and life prediction of an automotive adhesive bonding system. *Engineering Fracture Mechanics*, 2018; 189, 439–450.

31. Belnoue JPH, Giannis S, Dawson M, Hallett SR. Cohesive/adhesive failure interaction in ductile adhesive joints Part II: Quasi-static and fatigue analysis of double lap-joint specimens subjected to through-thickness compressive loading. *International Journal of Adhesion and Adhesives*, 2016; 68: 369–378.

32. de Moura MFSF, Gonçalves JPM. Cohesive zone model for high-cycle fatigue of composite bonded joints under mixed-mode I+ II loading. *Engineering Fracture Mechanics*, 2015; 140: 31–42.

33. Roe KL, Siegmund T. An irreversible cohesive zone model for interface fatigue crack growth simulation. *Engineering Fracture Mechanics*, 2003; 70(2): 209–232.

34. Khoramishad H, Crocombe AD, Katnam KB, Ashcroft IA. Predicting fatigue damage in adhesively bonded joints using a cohesive zone model. *International Journal of Fatigue*, 2010; 32(7): 1146–1158.

35. ISO B. 527-2: 1996. Plastics–determination of tensile properties–part 2: test conditions for moulding and extrusion plastics. *British Standards Institution*, 1996; 1–14.

36. ASTM D-3166-99: Standard test method for fatigue properties of adhesives in shear by tension loading (metal/metal). 2012.

37. Quaresimin M, Ricotta M. Fatigue behaviour and damage evolution of single lap bonded joints in composite material. *Composites Science and Technology*, 2006; 66(2), 176–187.

41

38. O'Mahoney DC, Katnam KB, O'Dowd NP, McCarthy CT, Young TM. Taguchi analysis of bonded composite single-lap joints using a combined interface–adhesive damage model. *International Journal of Adhesion and Adhesives*, 2013; 40, 168–178.

39. Shenoy V, Ashcroft IA, Critchlow GW, Crocombe AD, Wahab MA. An investigation into the crack initiation and propagation behaviour of bonded single-lap joints using backface strain. *International Journal of Adhesion and Adhesives*, 2009; 29(4), 361–371.

40. Huang L, Guo H, Shi Y, Huang S, Su X. Fatigue behavior and modeling of self-piercing riveted joints in aluminum alloy 6111. *International Journal of Fatigue*, 2017; 100, 274–284.

41. Wu G, Li D, Shi Y, Avery K, Huang L, Huang S, Su X, Peng Y. Stress Analysis on the Single-Lap SPR-Adhesive Hybrid Joint. *SAE Technical Paper*, 2018.

42. Hutchinson JW, Suo Z. Mixed mode cracking in layered materials. *Advances in Applied Mechanics*, 1991; 29: 63–191.

43. Suo Z. Delamination specimens for orthotropic materials. *Journal of Applied Mechanics*, 1990; 57(3): 627–634.